

Full-scale Representation Guided Network for Retinal Vessel Segmentation

Sunyong Seo, Huisu Yoon, Semin Kim, Jongha Lee
lululab Inc., AI R&D center
Seoul, 06054, Republic of Korea

{sy.seo, hs.yoon, sm.kim, jongha.lee}@lulu-lab.com

Abstract

The U-Net architecture and its variants have remained state-of-the-art (SOTA) for retinal vessel segmentation over the past decade. In this study, we introduce a Full Scale Guided Network (FSG-Net), where the feature representation network with modernized convolution blocks extracts full-scale information and the guided convolution block refines that information. Attention-guided filter is introduced to the guided convolution block under the interpretation that the filter behaves like the unsharp mask filter. Passing full-scale information to the attention block allows for the generation of improved attention maps, which are then passed to the attention-guided filter, resulting in performance enhancement of the segmentation network. The structure preceding the guided convolution block can be replaced by any U-Net variant, which enhances the scalability of the proposed approach. For a fair comparison, we re-implemented recent studies available in public repositories to evaluate their scalability and reproducibility. Our experiments also show that the proposed network demonstrates competitive results compared to current SOTA models on various public datasets. Ablation studies demonstrate that the proposed model is competitive with much smaller parameter sizes. Lastly, by applying the proposed model to facial wrinkle segmentation, we confirmed the potential for scalability to similar tasks in other domains. Our code is available on <https://github.com/ZombaSY/FSG-Net-pytorch>.

1. Introduction

Convolutional neural networks (CNNs) have seen significant improvements in performance and optimization since the 2010s. The introduction of hardware acceleration using GPUs, ReLU activation function, and residual block [11, 1] has enabled smooth back-propagation in deep neural network architectures. Research in this field has focused on finding a balance between computational efficiency, parameter size, code scalability, and fidelity. Depthwise separable

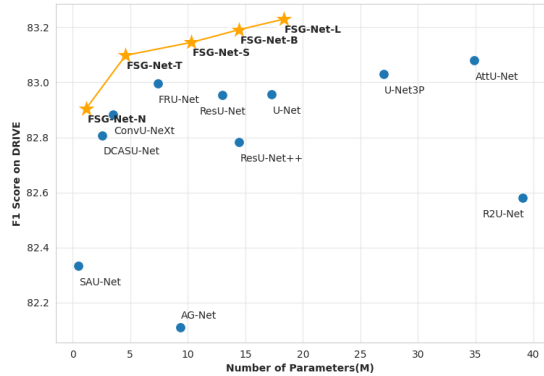


Figure 1. F1 scores of compared networks on the DRIVE dataset, measured against the validation dataset comprising zero-padded images of resolution 608×608 . Among the considered architectures, FSG-Net-T achieved a superior F1 score compared to competitive models while maintaining a reduced parameter size relative to its counterparts. Additionally, the FSG-Net-L achieved the highest F1 scores while possessing a median parameter size.

convolution [5] and squeeze-and-excitation [12] have been particularly influential in this regard. The inverted residual block [19] achieved higher fidelity with optimized computational efficiency and a smaller parameter size compared to ResNet.

In the evolutionary history of CNNs, a noteworthy highlight is the dominance of U-Net [18] and its variants [14, 21, 20, 28, 13, 8, 22] as SOTA models in the field of medical image segmentation, especially for retinal vessel segmentation tasks on well-known datasets such as DRIVE, STARE, CHASE_DB1, and HRF. On the contrary, for clinical segmentation tasks on the CVC-clinic and Kvasir-SEG datasets, vision transformer models are employed [23, 2, 3, 9]. The primary distinction between retinal vessels and other clinical datasets lies in the level of feature intricacy required. Vision transform models exhibit some limitations in overcoming their constrained inductive bias. Meanwhile, our experiments underscore the ongoing

relevance and effectiveness of attention mechanisms in addressing such challenges.

In this study, we aimed to propose a U-Net-based segmentation network that reflects the thin and elongated structural characteristics of retinal vessels, starting with the lower layers and gradually working our way up to the upper layers. Furthermore, based on the understanding that the guided filter [10] can function as a type of edge sharpening filter, the guided filter is located at the decoder after features from the encoder are merged so that full scale features can be used as input to the guided filters at each stage. Our network architecture improves both performance and computational efficiency simultaneously as shown in Figure 1. To ensure a fair comparison of the robustness of competing models, the training environment was maintained consistently.

The main contributions of this paper are summarized as follows: Firstly, enhancement of feature extraction through the proposal of a novel and efficient convolutional block. Secondly, proposing guided convolution blocks in the decoder, demonstrating performance enhancement as a result and enabling integration with various U-Net segmentation models. Thirdly, a comparison of various SOTA algorithms under a fixed experimental environment.

2. Method

2.1. Motivation

The guided filter was first introduced in [10] for image processing under the assumption that the guidance image and the filtered output have a locally linear relationship. The guided filter is formulated as:

$$\hat{I}_i = a_k I_i + b_k, \quad \forall i \in w_k, \quad (1)$$

where a, b are linear coefficients, and w is a local window. Here, we show why the guided filter can improve edge-like blood vessel segmentation performance. If we consider overlapping windows, the i -th pixel has several a_k and b_k values depending on the window size. Thus, the guided filter output of I_i can be averaged as follows:

$$\hat{I}_i = \frac{1}{|w|} \sum_{k \in w_i} (a_k I_i + b_k), \quad \forall i \in w_k. \quad (2)$$

Now, (2) can be rewritten to have a more intuitive form. In the original paper of the guided filter [10], b_k is computed as:

$$b_k = \bar{p}_k - a_k \bar{I}_k, \quad (3)$$

where $(\bar{\cdot})_k$ means average in w_k . Then, by putting Eq. (3) into Eq. (2), we have the following formulation:

$$\hat{I}_i = \bar{a}_i (I_i - \bar{I}_i) + \bar{p}_i, \quad (4)$$

where $(\bar{\cdot})_k$ denotes the average of the average, meaning $\bar{p}_i = \frac{1}{|w|} \sum_{k \in w_i} \bar{p}_k$. The unsharp mask filtering is defined as $\hat{I} = \alpha (I - L(I)) + I$, where $L(\cdot)$ is a low-pass filter such as the Gaussian filter. Eq. (4) looks like unsharpening mask filter, where sharpening mask $(I_i - \bar{I}_i)$ from the guidance image is added to the averaged target image. The filter strength is controlled by α .

In their pioneering work [26], Zhang et al. adopted the guided filter in the segmentation network and suggested incorporating the attention map M into the minimization problem to estimate a and b :

$$E(a_k, b_k) = \sum_{i \in w_k} \left(M_i^2 (a_k I_{di} + b_k - g_i)^2 + \mu a_k^2 \right). \quad (5)$$

In Eq. (5), the I_{di} is the downsampled input feature from encoding parts, and the g_i is the gating signal from upward path at the decoding parts. Eq. (5) implies that an improved attention map can lead to better solutions. In the following, we are going to propose a method that can generate an improved attention map with full-scale information.

2.2. Network architecture

As can be seen in Figure 2, the proposed network basically follows the U-Net architecture but has an additional guided convolution block after the feature representation network, unlike usual U-Net based structures. Contrary to the standard U-Net consisting of five stages, we have opted for four stages in FSG-Net based on the assumption that a wider receptive field is less critical for retinal vessel segmentation.

As described in the left part of FSG-Net, which is called the feature representation network, the input layer of the down-convolution is concatenated with a separate convolution from the other layers. These preserved features are then connected to the up-convolution layer. The deep bottleneck structure of the convolution block, indicated by the thick arrows, delivers a more enhanced feature representation. In the feature representation network, the key area to note is the feature merging section, indicated by the red dashed box. In this feature merging process, features from three paths—the current, upper, and lower stages—are concatenated and passed through a newly designed convolution block before being forwarded to the subsequent stages. This approach allows the integration and transmission of information across all scales.

In the right part of the model, namely the guided convolution block, compressed features reflecting full scale information are given as the current stage input to the guided residual module (GRM). Up-stage input from the higher stage is given as another input for guided filtering. After GRM, predictions are derived through convolution and activation. For training, a combination of the dice loss and

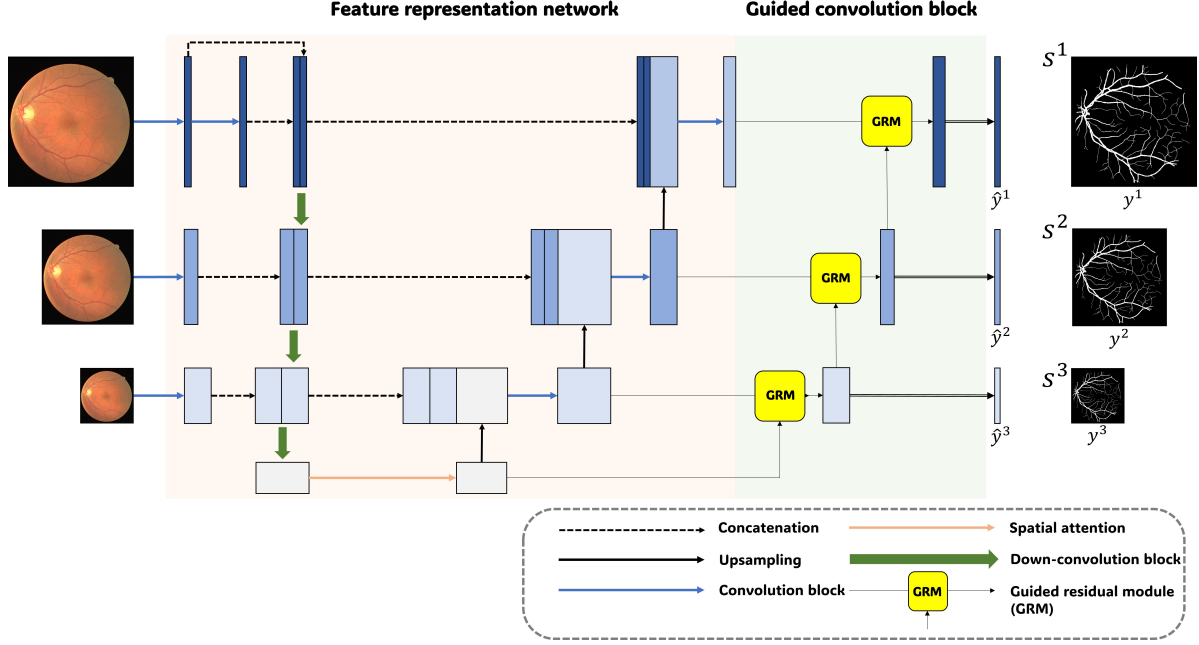


Figure 2. Network architecture of the proposed FSG-Net.

BCE loss was employed to improve segmentation performance of the edge-like structures [7]:

$$L_{DS} = \sum_{d=1}^D \sum_{i=0}^{S^d} (y_i \log \hat{y}_i^d + (1 - y_i) \log(1 - \hat{y}_i^d)), \quad (6)$$

$$L_{Dice} = 1 - \sum_{d=1}^D \sum_{i=1}^{S^d} \frac{2(y_i \cdot \hat{y}_i^{(d)})}{y_i + \hat{y}_i^{(d)} + \epsilon}, \quad (7)$$

$$L_{total} = L_{DS} + L_{Dice}, \quad (8)$$

where S denotes the indices and L_{Dice} for Dice loss over pixels. For deep-supervision, D represents the number of layers, the prediction at layer d , and weights for each layer, respectively.

Lastly, we can consider the scalability of the proposed architecture. The feature representation network can be replaced by other U-Net variants, enabling integration with the guided convolution block. For instance, we can consider integrating with FR-UNet [15], which proposes alternative methods for utilizing full-scale information.

2.3. Modernized convolution block

The standard U-Net has a fundamental structure comprising skip connections and double convolution blocks. Recent studies have shown that incorporating different CNN structures can significantly improve the performance

of the original model [16, 9]. Inspired by the ConvNeXt [16], we have designed a convolutional block suitable for retinal vessel segmentation.

Figure 3(a) and (b) represent the depthwise residual block and inverted residual block, respectively. Figure 3(c) shows the proposed convolution block. The structure of the block is an extension of the latest advancements in convolutional block development, characterized by features such as 1×1 convolution, inverted bottleneck, and depth-wise convolution. Like other modernized convolution blocks, the proposed block employs a convolution with kernel size 2 and stride 2 in the first stage. By incorporating spatial and dimensional changes within the first block, we enable the design of a deep bottleneck stage in the down-convolution structure. This approach not only increases the information on the feature but also separates it from the bottleneck, allowing for more detailed feature representation. Furthermore, to maintain linearity, we utilize unique ReLU activation between each inverted residual block. For regularization purposes, we employ a learnable gamma parameter and apply a drop block before joining the identity block.

2.4. Guided convolution block

As shown in Figure 2, the guided convolution block consists of GRM to refine the input from the feature representation network and a convolution to output the prediction map. Figure 4 shows the overall process of GRM. The purpose of GRM is to refine the feature from the feature representation network at the same stage. In GRM, both the features at the current stage and at the higher stage are used

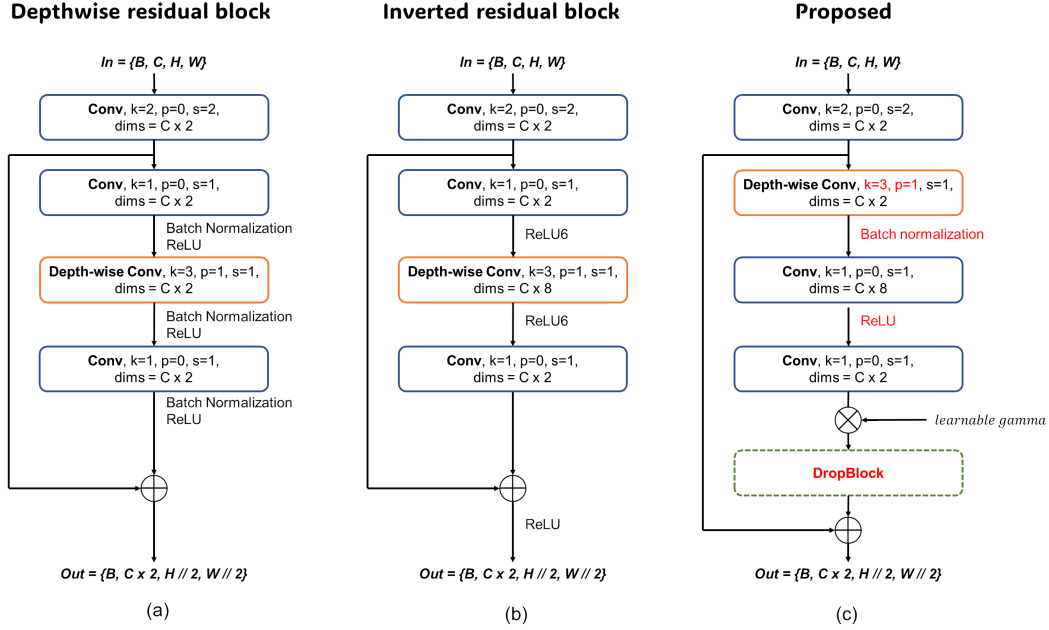


Figure 3. The evolutionary structure from (a): Depthwise residual block, (b): Inverted residual block to (c): The proposed convolution block.

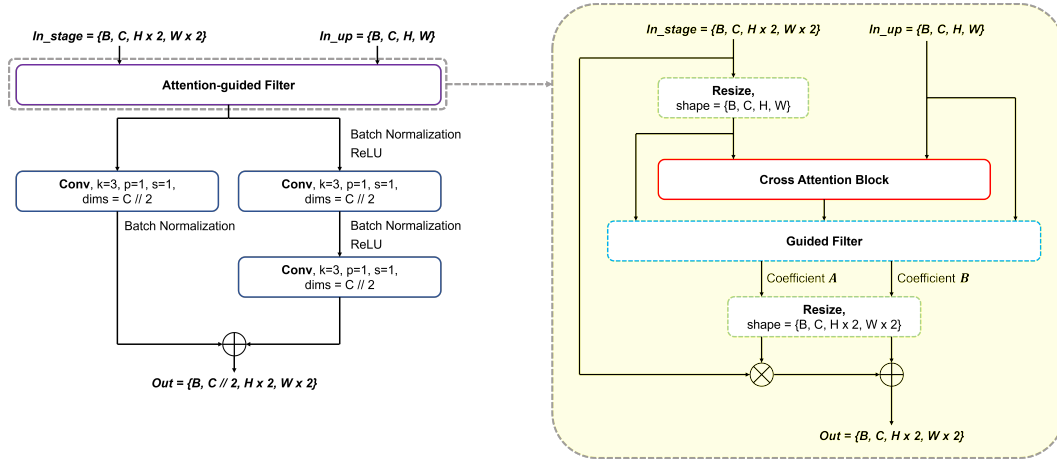


Figure 4. Detailed structure of guided residual module (GRM)

to generate an attention map, and then the attention map is multiplied with the current feature to generate the output, which is described in the right part of Figure 4. Here we can expect an improved attention map M can be estimated to solve Eq. (5) because the input feature from the feature representation network has full scale information. To further enhance the feature refinement, a residual block is introduced after the attention-guided filtering, as shown in the left part of Figure 4. By passing the features through the residual block, a stable map is generated for both the deep supervision and subsequent layers. Moreover, we incorporate a 1×1 convolution to preserve the semantic information present in the feature maps.

3. Experiments

3.1. Training Techniques

In retinal vessel segmentation, the performance of studies is often determined by subtle gaps. We believe that these subtle gaps are highly influenced by the choice of hyperparameters and training/inference environment. To address this imbalance, we fixed all hyperparameters for training and inference. We empirically found that RandAugment [6] with a specific scale did not work well on medical datasets; therefore, we customized it to better suit our datasets. Training techniques include blur, color jitter, horizontal flip, perspective transformation, resize, crop, and CutMix [25].

Table 1. Train settings and hyper-parameters.

Hyper-parameters	Values
base lr	1e-3
lr scheduler	Cosine annealing
lr scheduler warm-up epochs	20
lr scheduler cycle epochs	100
lr scheduler eta min	1e-5
early stop epochs	400
early stop metric	F1 score
optimizer	AdamW
optimizer momentum	$\beta_1, \beta_2=0.9, 0.999$
weight decay	0.05
criterion	Dice + BCE
binary threshold	0.5
batch size	4
random crop	288
random blur	prob=0.8
random jitter	prob=0.8
random horizontal flip	prob=0.5
random perspective	prob=0.3
random random resize	prob=0.8
CutMix	n=1, prob=0.8

3.2. Implementation Details

Our experimental environment comprises an Intel Xeon Gold 5220 processor, a Tesla V100-SXM2-32GB GPU, Pytorch 1.13.1, and CUDA version 11.7. The inference time for FSG-Net-L was approximately $600ms$ for an input size of (608, 608) using a GPU-synchronized flow. To address as much variability as possible, we re-implemented comparison studies and integrated them into a single environment. To ensure experimental fairness, certain hyperparameters, including the framework, loss function, metric, data augmentation, and random seed, were fixed to measure the robustness of the model. Our training settings followed the hyperparameters in Table 1, used for segmentation tasks in ADE20K multiscale learning in ConvNeXt [16].

To evaluate the compared models under the same conditions, we prioritized the search for an optimized model in our training settings. For example, the learning rate can affect the gradient updating and training time, depending on the model’s parameter size and depth. Training for a predetermined number of epochs can result in diverging weights for heavy models and, conversely, for light models. Therefore, we chose the optimized model using an early stop based on cycles in the learning rate scheduler. To select the optimized model during the training step, we used the highest F1 score [27], with an early stop of 400 epochs. To balance exploitation and exploration in the learning parameters, we stack the batch to have more than two sets of mini-batches in one epoch with a learning rate scheduler. The detailed hyper-parameters are described in Table 1. With these experimental settings, the performance of the pure U-Net dramatically increased and even surpassed that of some recent studies, as shown in Table 2.

3.3. Datasets

The DRIVE dataset comprised 40 retinal images with a resolution of 565×584 pixels, captured as part of a retinopathy screening study in the Netherlands. The STARE dataset comprises 20 retinal fundus images with a resolution of 700×605 pixels, and the CHASE_DB1 dataset includes 28 retinal images from schoolchildren with a resolution of 999×960 pixels. Both the STARE and CHASE_DB1 datasets were manually annotated by two independent experts. We used the annotation of the first expert, named "Hoover A." in STARE and "1stHO" in CHASE_DB1, for our analysis. The HRF dataset comprises 45 images, equally divided into a 1:1:1 ratio of healthy patients, diabetic retinopaths, and glaucomatous patients, with a high resolution of 3504×2336 pixels. To measure the performance of the models, it is necessary to divide the data into training and validation sets. As the retinal vessel segmentation dataset was relatively limited, we split the data into a 1:1 ratio of the training and validation sets. The DRIVE dataset was officially divided into training and validation sets, each containing 20 images. For the STARE, CHASE_DB1, and HRF datasets, we used the first half as training and the remaining half as validation.

3.4. Results

In binary task evaluations, the Matthew correlation coefficient (MCC) is a powerful metric, as noted by Chicco *et al.* [4]. However, to avoid evaluations oriented towards a specific metric, we also report the average rank of each model, denoted as "Rank Avg" in Table 2. This average rank provides a measure of the stable performance of a model across different datasets. For example, FSG-Net, U-Net3+ [13], and AttU-Net [17] achieved high ranks in all three datasets, whereas ResU-Net and FR-UNet recorded inconsistent results across the three datasets. FSG-Net achieved the highest rank in terms of performance across all three datasets, recording dominant scores in mIoU, F1 score, and MCC, which is equivalent to a detailed expression of the segmentation map. Notably, FSG-Net outperformed the DRIVE dataset, recording SOTA in the F1 score and sensitivity. Figure 5 represents the predicted segmentation maps of the three best models in our evaluation metrics. The FSG-Net shows the best results, especially in segmenting thin vessels. FSG-Net incorporates deep supervision, which allows for the extraction of segmentation maps at each stage. Figure 6 shows the vessel detection results at various stages. It can be observed that as we move to lower levels, the performance in detecting thinner vessels improves. An interesting point is that even at coarse stage S_3 , the detection of thicker vessels is generally well-maintained.

In the inference settings, we padded the original image with a multiple of 32 to preserve the flexible operation of

Table 2. Metric comparison of results on datasets.

Architecture	mIoU	F1 score	Acc	AUC	Sen	MCC	Rank Avg
DRIVE							
U-Net	83.857	82.956	97.013	97.853	83.449	81.456	5
U-Net++	81.228	79.564	96.524	96.271	77.802	77.830	13
U-Net3+ Deep	83.909	83.030	97.017	98.082	83.721	81.520	3.1
ResU-Net	83.862	82.953	97.021	97.766	83.226	81.453	5.8
ResU-Net++	83.729	82.783	97.001	97.708	82.791	81.263	9.1
SAU-Net	83.368	82.334	96.925	97.616	82.311	80.782	11.2
DCASU-Net	83.743	82.808	96.996	97.838	83.080	81.290	7.8
AG-Net	83.176	82.111	96.882	97.628	82.155	80.540	11.8
AttU-Net	83.958	83.080	97.039	97.844	83.422	81.584	3.2
R2U-Net	83.555	82.580	96.952	97.879	82.961	81.038	8.8
ConvU-NeXt	83.800	82.882	97.012	97.835	83.019	81.367	7.2
FR-UNet	83.884	82.995	97.007	98.158	83.869	81.485	3.8
FSG-Net-L (ours)	84.068	83.229	97.042	98.235	84.207	81.731	1
STARE							
U-Net	85.924	84.873	97.754	98.341	84.361	83.713	3.3
U-Net++	81.514	79.061	97.022	94.479	75.539	77.764	12.8
U-Net3+ Deep	85.824	84.829	97.707	99.146	85.522	83.626	3.5
ResU-Net	85.964	84.872	97.767	98.050	83.997	83.726	3.5
ResU-Net++	83.185	81.358	97.319	95.221	78.456	80.196	11.7
SAU-Net	85.158	84.061	97.604	97.784	84.015	82.885	7
DCASU-Net	84.423	83.064	97.454	98.362	83.583	81.771	8.8
AG-Net	84.811	83.766	97.565	98.403	83.347	82.516	7.7
AttU-Net	85.848	84.772	97.694	99.050	86.226	83.588	3.8
R2U-Net	83.727	81.786	97.468	93.457	77.048	80.810	11.3
ConvU-NeXt	85.339	84.186	97.658	97.866	83.401	82.998	6.7
FR-UNet	84.815	83.496	97.577	96.637	81.872	82.327	9.2
FSG-Net-L (ours)	86.118	85.100	97.746	98.967	86.608	83.958	1.7
CHASE_DB1							
U-Net	82.065	80.159	97.404	99.368	85.370	79.002	6
U-Net++	81.512	79.415	97.321	99.362	84.143	78.201	8.2
U-Net3+ Deep	82.489	80.697	97.483	99.506	85.740	79.558	2.7
ResU-Net	81.104	78.810	97.320	99.278	81.311	77.479	11.5
ResU-Net++	73.276	67.411	95.966	96.223	67.782	65.593	13
SAU-Net	81.335	79.100	97.338	99.407	82.265	77.802	8.8
DCASU-Net	82.254	80.368	97.483	99.329	83.916	79.161	5.3
AG-Net	82.158	80.272	97.440	99.544	84.817	79.070	4.2
AttU-Net	82.562	80.742	97.546	99.430	83.907	79.537	3.3
R2U-Net	81.250	78.944	97.384	98.792	80.054	77.625	10.8
ConvU-NeXt	81.752	79.704	97.405	99.402	83.009	78.439	7
FR-UNet	81.330	79.170	97.269	99.544	84.744	77.944	7.7
FSG-Net-L (ours)	82.680	81.019	97.515	99.378	85.995	79.899	2.2
HRF							
U-Net	82.291	81.329	97.093	98.571	82.756	79.868	4.8
U-Net++	82.653	80.995	97.040	98.450	82.402	79.522	7.6
U-Net3+ Deep	83.006	81.445	97.124	98.427	82.436	79.997	4.1
ResU-Net	82.908	81.299	97.098	98.415	82.481	79.842	6.8
ResU-Net++	77.008	73.096	96.032	95.312	70.587	71.251	12.8
SAU-Net	82.015	80.170	96.892	98.539	82.195	78.624	9.5
DCASU-Net	82.942	71.335	97.109	98.499	82.383	79.884	7.0
AG-Net	82.249	80.474	96.961	98.566	81.810	78.951	8.6
AttU-Net	83.017	81.448	97.113	98.558	82.830	79.996	2.6
R2U-Net	80.998	78.699	96.808	96.976	77.231	77.122	11.8
ConvU-NeXt	83.015	81.423	97.121	98.525	82.520	79.974	3.8
FR-UNet	82.431	80.709	97.011	98.294	81.677	79.218	9.5
FSG-Net-L (ours)	83.088	81.567	97.106	98.744	83.616	80.121	1.6

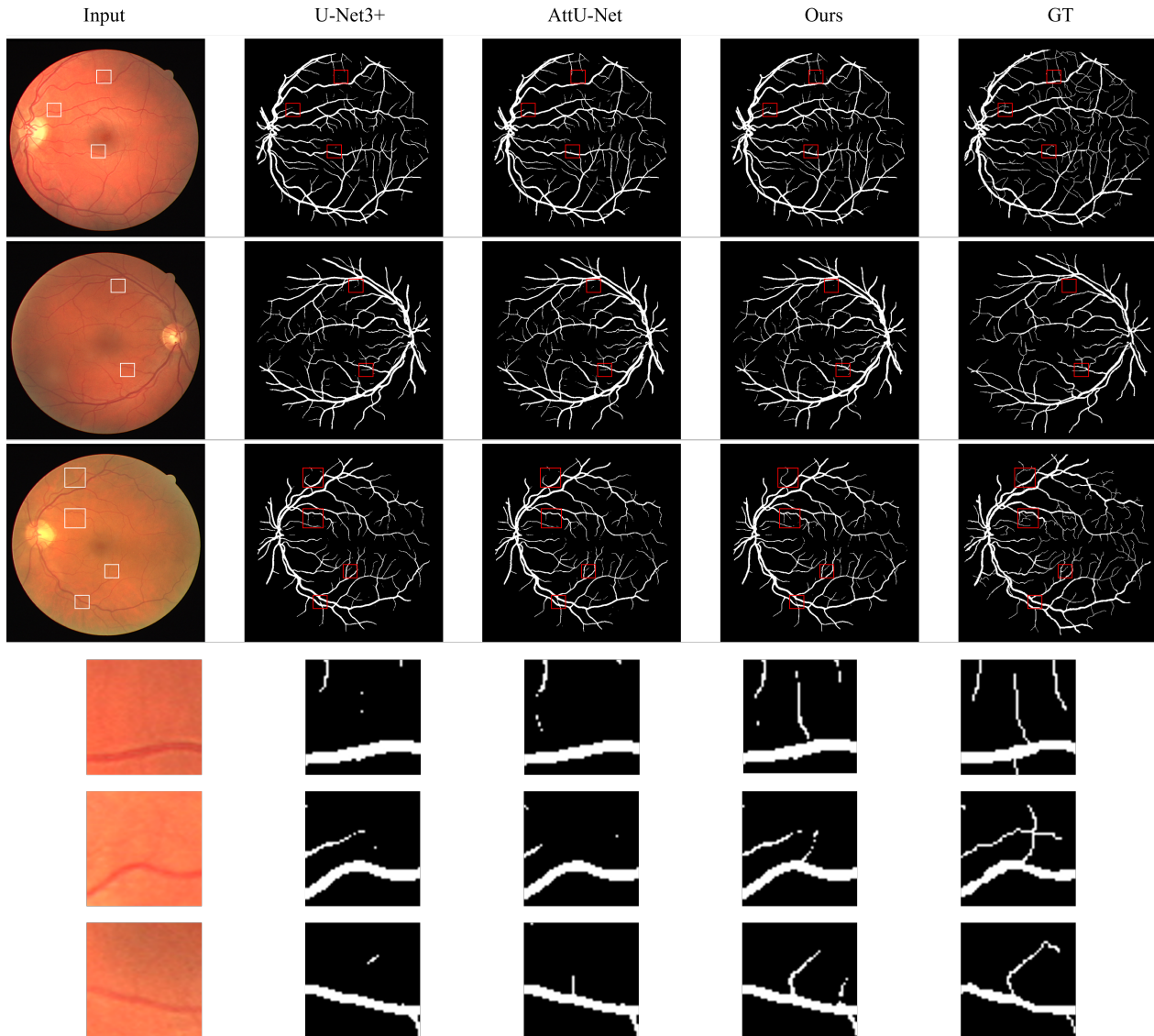


Figure 5. Qualitative evaluation on top-3 model structure on DRIVE validation set.

specific models. Resizing the shape can lead to informational loss, which is critical in retinal vessel segmentation that requires high-fidelity maps. When measuring the metrics, we again removed the padding to generate a perfectly similar shape to the original image with no informational loss. With this unpadding trick, metrics that require true negatives and false negatives can be decreased compared with padded or resized images. Remarkably, the majority of models examined in our study exhibited superior performance compared to their original implementations in our training settings. For example, AG-Net achieved better performance on the DRIVE dataset (cIoU:69.71, Sen:82.16) in our environment than the results reported in the original paper (cIoU:69.65, Sen:81.00). Furthermore, U-Net, despite being an early model introduced over a decade ago, demon-

strated robustness by achieving middle-range performance using only pure convolution layers.

3.5. Ablation study

To further understand the impact of the model capacity and structure on FSG-Net, we conducted ablation studies. In Table 3, we vary the depth of the down-convolution, base channel (Base_c) and structure. The F1 score of three datasets is used as a metric here. The results showed that even the smallest version of FSG-Net surpassed the other models. By comparing the scores in Table 2, the smallest FSG-Net with 1.17M parameters outperformed recent studies with an average rank of 5.2 across all metrics on the three datasets, compared to SAU-Net’s rank of 9.0 with a parameter size of 0.5M, DCASU-Net’s [24] rank of 7.0 with a

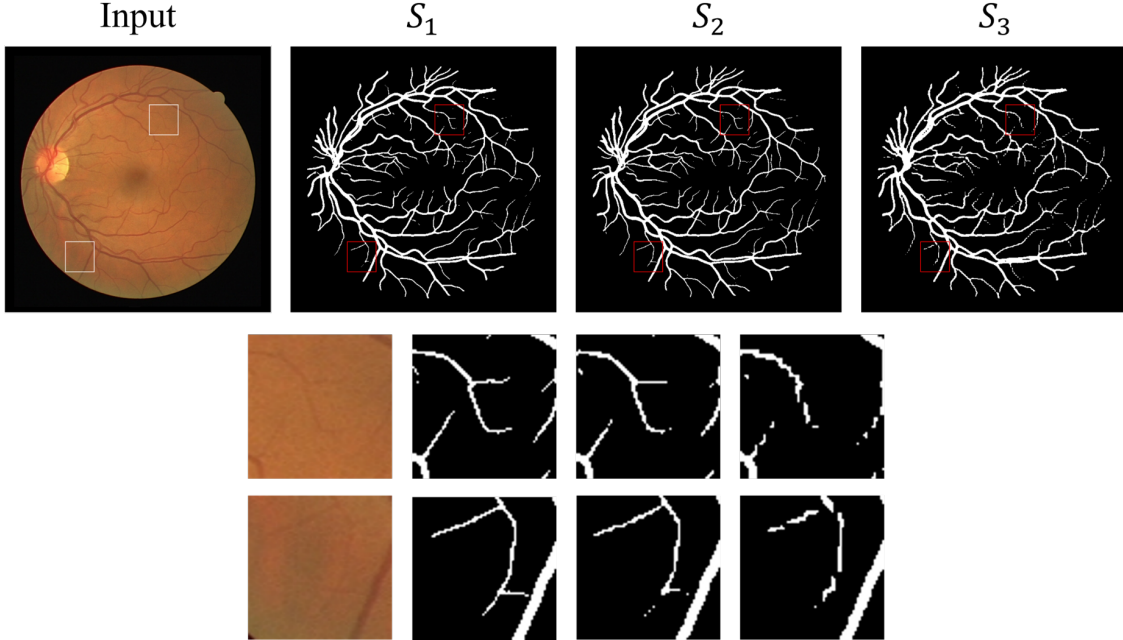


Figure 6. Inspection on output map at each stage S_i on FSG-Net. The finer scale of map describes more detailed lines.

parameter size of 2.6M, ConvU-NeXt’s rank of 6.7 with a parameter size of 3.5M, and FR-UNet’s rank of 6.6 with a parameter size of 7.4M.

Table 3. Ablation studies on model capacity and model structure

model	Base_c	Depth	Params (M)	DRIVE	STARE	CHASE_DB1
FSG-Net-L	64	[3, 3, 9, 3]	18.32	83.229	85.100	81.019
FSG-Net-B	64	[2, 2, 6, 2]	14.46	83.191	84.934	79.658
FSG-Net-S	48	[3, 3, 9, 3]	10.33	83.145	84.917	80.529
FSG-Net-T	32	[3, 3, 9, 3]	4.61	83.098	84.698	79.982
FSG-Net-N	16	[3, 3, 9, 3]	1.17	82.904	84.692	79.431
Structure						
kernel size 3 to 7			35.77	83.006	84.200	80.044
AGF to AttU-Net like			19.61	83.115	84.671	79.333
down-conv to residual			45.60	82.893	82.734	75.765
w/o deep supervision			18.32	83.131	84.698	79.889
removing spatial attention			18.32	83.237	84.598	79.946

To optimize the network structure, we investigated the impact of increasing the kernel size, replacing the attention-guided filter with a simple attention block, and the effect of using pure residual blocks or removing the spatial attention. Our findings show that while increasing the kernel size expands the receptive field, it fails to improve performance in retinal vessel segmentation tasks that require detailed expression of the segmentation map. We found that the attention-guided filter proved to be robust and effective for this task. Additionally, we observed that using pure residual blocks in the deep bottleneck stage increases the parameter size and reduces computational efficiency without significantly improving feature extraction. Removing the spatial attention improved the performance in the DRIVE dataset; however, as the input size increased, the performance decreased proportionally.

4. Discussion

We previously emphasized the method of feature merging within the network architecture. This is because feature merging allows information from all stages to be mixed and provided as input to the guided filtering module. This approach can be compared to AG-Net, which also gathers features and provides them to the guided filter. Figure 7(a) illustrates the feature merging in the proposed method, while Figure 7(b) shows the corresponding part of AG-Net. Let us focus on the left path to the guided filtering modules in both cases. As can be seen in Figure 7(a), feature maps from three stages (current, upward, and downward) are concatenated and passed through the proposed convolution block. For AG-Net, only the features from the current and lower stages are merged for the attention-guided filter. In summary, our GRM gets feature information from all stages with a modernized convolution, while the AG-Net gets it from current and lower stages with conventional convolutions. For this reason, we were able to achieve superior performance with one fewer stage than AG-Net.

The next discussion point concerns the experimental datasets. DRIVE, STARE, and Chase_DB1 are representative datasets for retinal vessel segmentation. Models that improve the architecture of layers and attention mechanisms continue to emerge, but the number of images in such datasets is limited. Although this paper focuses on retinal vessel segmentation, it is necessary to apply the proposed model to large databases from other fields to verify its variability and scalability. In our future work, we can consider

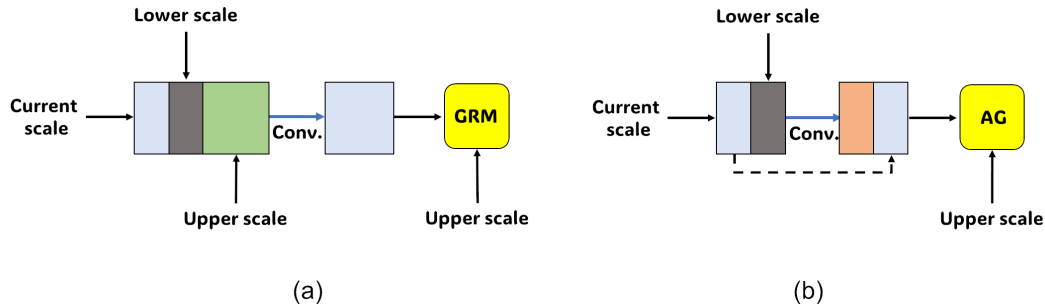


Figure 7. Compared structure of feature merging in (a) FSG-Net, and (b) AG-Net.

expanding our application areas to include crack detection, facial wrinkle detection, and general medical imaging.

5. Conclusion

In this study, we presented a full-scale representation guided network for retinal vessel segmentation that achieves SOTA on the DRIVE dataset. A modern convolutional block tailored for retinal vessel segmentation was designed, and the guided convolution block maximized performance using full-scale information from the feature representation network. The proposed guided convolution block is compatible with any U-Net architecture, offering scalability for similar tasks across various domains. We encourage future research to use the FSG-Net architecture and our experimental settings to ensure reproducibility and scalability in similar tasks.

References

- [1] Md Zahangir Alom, Mahmudul Hasan, Chris Yakopcic, Tarek M. Taha, and Vijayan K. Asari. Recurrent residual convolutional neural network based on u-net (r2u-net) for medical image segmentation, 2018.
- [2] Hu Cao, Yueyue Wang, Joy Chen, Dongsheng Jiang, Xiaopeng Zhang, Qi Tian, and Manning Wang. Swin-unet: Unet-like pure transformer for medical image segmentation. In Leonid Karlinsky, Tomer Michaeli, and Ko Nishino, editors, *Computer Vision – ECCV 2022 Workshops*, pages 205–218, Cham, 2023. Springer Nature Switzerland.
- [3] Jieneng Chen, Yongyi Lu, Qihang Yu, Xiangde Luo, Ehsan Adeli, Yan Wang, Le Lu, Alan L. Yuille, and Yuyin Zhou. Transunet: Transformers make strong encoders for medical image segmentation, 2021.
- [4] Davide Chicco, Valery V. Starovoitov, and Giuseppe Jurman. The benefits of the matthews correlation coefficient (mcc) over the diagnostic odds ratio (dor) in binary classification assessment. *IEEE Access*, 9:47112–47124, 2021.
- [5] Francois Chollet. Xception: Deep learning with depthwise separable convolutions. In *Proceedings of the IEEE Conference on Computer Vision and Pattern Recognition (CVPR)*, July 2017.
- [6] Ekin D. Cubuk, Barret Zoph, Jonathon Shlens, and Quoc V. Le. Randaugment: Practical automated data augmentation with a reduced search space. In *Proceedings of the IEEE/CVF Conference on Computer Vision and Pattern Recognition (CVPR) Workshops*, June 2020.
- [7] Lu Deng, An Zhang, Jingjing Guo, and Yingkai Liu. An integrated method for road crack segmentation and surface feature quantification under complex backgrounds. *Remote Sensing*, 15(6), 2023.
- [8] Changlu Guo, Márton Szemenyei, Yugen Yi, Wenle Wang, Buer Chen, and Changqi Fan. Sa-unet: Spatial attention u-net for retinal vessel segmentation. In *2020 25th International Conference on Pattern Recognition (ICPR)*, pages 1236–1242, 2021.
- [9] Zhimeng Han, Muwei Jian, and Gai-Ge Wang. Convunext: An efficient convolution neural network for medical image segmentation. *Knowledge-Based Systems*, 253:109512, 2022.
- [10] Kaiming He, Jian Sun, and Xiaoou Tang. Guided image filtering. *IEEE Transactions on Pattern Analysis and Machine Intelligence*, 35(6):1397–1409, 2013.
- [11] Kaiming He, Xiangyu Zhang, Shaoqing Ren, and Jian Sun. Deep residual learning for image recognition. In *Proceedings of the IEEE Conference on Computer Vision and Pattern Recognition (CVPR)*, June 2016.
- [12] Jie Hu, Li Shen, and Gang Sun. Squeeze-and-excitation networks. In *Proceedings of the IEEE Conference on Computer Vision and Pattern Recognition (CVPR)*, June 2018.
- [13] Huimin Huang, Lanfen Lin, Ruofeng Tong, Hongjie Hu, Qiaowei Zhang, Yutaro Iwamoto, Xianhua Han, Yen-Wei Chen, and Jian Wu. Unet 3+: A full-scale connected unet for medical image segmentation. In *ICASSP 2020 - 2020 IEEE International Conference on Acoustics, Speech and Signal Processing (ICASSP)*, pages 1055–1059, 2020.
- [14] Debesh Jha, Pia H. Smedsrud, Michael A. Riegler, Dag Johansen, Thomas De Lange, Pål Halvorsen, and Håvard D. Johansen. Resunet++: An advanced architecture for medical image segmentation. In *2019 IEEE International Symposium on Multimedia (ISM)*, pages 225–2255, 2019.
- [15] Wentao Liu, Huihua Yang, Tong Tian, Zhiwei Cao, Xipeng Pan, Weijin Xu, Yang Jin, and Feng Gao. Full-resolution network and dual-threshold iteration for retinal vessel and coronary angiograph segmentation. *IEEE Journal of Biomedical and Health Informatics*, 26(9):4623–4634, 2022.

- [16] Zhuang Liu, Hanzi Mao, Chao-Yuan Wu, Christoph Feichtenhof, Trevor Darrell, and Saining Xie. A convnet for the 2020s. In *Proceedings of the IEEE/CVF conference on computer vision and pattern recognition*, pages 11976–11986, 2022.
- [17] Ozan Oktay, Jo Schlemper, Loïc Le Folgoc, Matthew C. H. Lee, Mattias P. Heinrich, Kazunari Misawa, Kensaku Mori, Steven G. McDonagh, Nils Y. Hammerla, Bernhard Kainz, Ben Glocker, and Daniel Rueckert. Attention u-net: Learning where to look for the pancreas. *CoRR*, abs/1804.03999, 2018.
- [18] Olaf Ronneberger, Philipp Fischer, and Thomas Brox. U-net: Convolutional networks for biomedical image segmentation. In Nassir Navab, Joachim Hornegger, William M. Wells, and Alejandro F. Frangi, editors, *Medical Image Computing and Computer-Assisted Intervention – MICCAI 2015*, pages 234–241, Cham, 2015. Springer International Publishing.
- [19] Mark Sandler, Andrew Howard, Menglong Zhu, Andrey Zhmoginov, and Liang-Chieh Chen. Mobilenetv2: Inverted residuals and linear bottlenecks. In *Proceedings of the IEEE Conference on Computer Vision and Pattern Recognition (CVPR)*, June 2018.
- [20] Nahian Siddique, Sidike Paheding, Colin P. Elkin, and Vijay Devabhaktuni. U-net and its variants for medical image segmentation: A review of theory and applications. *IEEE Access*, 9:82031–82057, 2021.
- [21] Yucheng Tang, Dong Yang, Wenqi Li, Holger R. Roth, Bennett Landman, Daguang Xu, Vishwesh Nath, and Ali Hatamizadeh. Self-supervised pre-training of swin transformers for 3d medical image analysis. In *Proceedings of the IEEE/CVF Conference on Computer Vision and Pattern Recognition (CVPR)*, pages 20730–20740, June 2022.
- [22] Chunwei Tian, Yong Xu, Zuoyong Li, Wangmeng Zuo, Lunke Fei, and Hong Liu. Attention-guided cnn for image denoising. *Neural Networks*, 124:117–129, 2020.
- [23] Enze Xie, Wenhai Wang, Zhiding Yu, Anima Anandkumar, Jose M Alvarez, and Ping Luo. Segformer: Simple and efficient design for semantic segmentation with transformers. *Advances in neural information processing systems*, 34:12077–12090, 2021.
- [24] Qing Xu, Zhicheng Ma, Na HE, and Wenting Duan. Dcsaunet: A deeper and more compact split-attention u-net for medical image segmentation, 2022.
- [25] Sangdoon Yun, Dongyoon Han, Seong Joon Oh, Sanghyuk Chun, Junsuk Choe, and Youngjoon Yoo. Cutmix: Regularization strategy to train strong classifiers with localizable features. In *Proceedings of the IEEE/CVF International Conference on Computer Vision (ICCV)*, October 2019.
- [26] Shihao Zhang, Huazhu Fu, Yuguang Yan, Yubing Zhang, Qingyao Wu, Ming Yang, Minghui Tan, and Yanwu Xu. Attention guided network for retinal image segmentation. In Dinggang Shen, Tianming Liu, Terry M. Peters, Lawrence H. Staib, Caroline Essert, Sean Zhou, Pew-Thian Yap, and Ali Khan, editors, *Medical Image Computing and Computer Assisted Intervention – MICCAI 2019*, pages 797–805, Cham, 2019. Springer International Publishing.
- [27] Zhengxin Zhang, Qingjie Liu, and Yunhong Wang. Road extraction by deep residual u-net. *IEEE Geoscience and Remote Sensing Letters*, 15(5):749–753, 2018.
- [28] Zongwei Zhou, Md Mahfuzur Rahman Siddiquee, Nima Tajbakhsh, and Jianming Liang. Unet++: A nested u-net architecture for medical image segmentation. In Danail Stoyanov, Zeike Taylor, Gustavo Carneiro, Tanveer Syeda-Mahmood, Anne Martel, Lena Maier-Hein, João Manuel R.S. Tavares, Andrew Bradley, João Paulo Papa, Vasileios Belagiannis, Jacinto C. Nascimento, Zhi Lu, Sailesh Conjeti, Mehdi Moradi, Hayit Greenspan, and Anant Madabhushi, editors, *Deep Learning in Medical Image Analysis and Multimodal Learning for Clinical Decision Support*, pages 3–11, Cham, 2018. Springer International Publishing.